ELSEVIER

PII: S0955-7997(97)00005-2

*Engineering Analysis with Boundary Elements* **19** (1997) 181–198

0955-7997/97/$17.00

# Harmonic elastic waves in continuously heterogeneous random layers

**G. D. Manolis**

*Aristotle University, Dept. of Civil Engineering, Thessaloniki 54006, Greece*

&

**R. P. Shaw**

*SUNY at Buffalo, Dept. of Civil Engineering, Buffalo, New York 14260, USA*

(Received 1 March 1996; revised 24 April 1996; accepted 24 April 1996)

Solutions for one dimensional elastic waves in a continuously heterogeneous layer are derived under fairly general material parameter constraints. These solutions are further developed for the case corresponding to horizontally polarized shear wave propagation under time harmonic conditions and a versatile Green's function due to a point source is derived, which includes material damping and the presence of a traction-free horizontal surface. Subsequently, randomness in the layer's material parameters is introduced and the perturbation technique is used for deriving mean values and covariances for the Green's function. Through a series of numerical example, this Green's function approach is contrasted with conventional formulations for layered media employing transfer matrix techniques. The present approach is shown to be an efficient alternative which can be used not only in conjunction with boundary element formulations for wave scattering problems, but also in spectral representations of waves propagating through layered media. © 1997 Elsevier Science Ltd

*Key words:* Heterogeneity, fundamental solutions, layered media, random media, wave propagation.

## INTRODUCTION

The propagation of waves in naturally occurring media is the theoretical cornerstone of many diverse fields such as seismology and earthquake engineering, acoustic and electromagnetic signal transmission, noise control, subsurface exploration, etc. Since the focus of the present work is one dimensional wave propagation in a continuously inhomogeneous and stochastic layer, the most closely related field of application is seismically-induced ground motions on the earth's surface. The estimation of ground shaking at a particular site is, at present, an open problem as discussed in Bard,[1] but its importance in earthquake hazard mitigation and earthquake resistant design is paramount.

It is well known that local geological structure plays an important role on the resulting seismic motions[2] and recent major earthquakes have all provided fresh evidence of this. The basic approaches for estimation of site effects (excluding statistical techniques aimed at assessing certain gross site characteristics) can be classified as follows: (i) instrument recordings which produce measurements that are either reference site specific or reference site independent.[3] In addition, there exist microtremor recordings, especially in Japan, but their use remains controversial[1] since it is difficult to discriminate seismic source effects from local site effects; (ii) analytical/numerical methods have been extensively used in recent years[4] and are continuously developed in view of rapid advances in electronic computer technology. Four basic categories can be distinguished, namely theoretical solutions which may be used for a limited number of problems, ray methods which are essential high frequency approximations, boundary techniques such as boundary integrals, boundary elements and wave function expansions and finally domain techniques such as finite elements and finite differences. All these methods have their advantages and disadvantages and each of them can be effectively applied to a certain range or

class of problems (e.g. Refs 5–10); (iii) physical modelling, with very few exceptions, is basically underdeveloped probably because of economic reasons. It seems possible, however, to conduct site response tests within the context of shaking table and pseudodynamic tests currently performed for earthquake engineering studies.[11]

The factors which influence site effects are numerous but the most important ones appear to be the following: (i) surface topography, which can be classified into 'convex' (hills, cliff borders) and 'concave' (valleys, foothills). This change from conventional smooth, rolling topography produces seismic motion amplification at the crests and deamplification at the troughs and the wave mechanisms responsible are diffraction, focusing/defocusing and incident angle sensitivity;[12–14] (ii) nonlinear behavior of soft soil deposits, which can be classified as either sand or clay, when peak ground accelerations are in the range 0·1–0·3 g or higher;[15–17] (iii) trapping of seismic energy in soft layers bounded by stiff layers, which leads to increased amplification and is due to wave diffraction by subsurface topography;[2] (iv) ground failures such as liquefaction and earthquake-triggered landslides can have very important consequences in earthquake engineering, but their underlying physical mechanisms are very different and have little to do with wave propagation; (iv) soil–structure interaction is a rather localized phenomenon which depends on the presence of large-size structures or massive ones built on soft soil deposits;[18] (v) various phenomena associated with the general propagation of seismic waves as they travel through soil layers (such as geometric spreading, absorption, dispersion, energy reflection, refraction and diffraction) which are due to soil heterogeneity, layering, the presence of discontinuities or gross impurities, the presence of a second phase in the ground such as water and general randomness in the structure of the soil, all contribute in modifying the seismic signals emanating from bedrock.[19–23] Implicit in the study of these phenomena is the ability to produce an accurate description of the soil's properties based on *in-situ* or laboratory testing.[23–25]

Local site effects and the study of seismic wave propagation through soil forms the link between seismology and earthquake engineering. Furthermore, the influence of the last few hundred meters of soil in modifying incoming earthquake signals (that can be recorded at rock outcroppings) is beyond dispute and all recent destructive earthquakes have confirmed it. It is therefore necessary to continue the development of wave propagation models through layered (e.g. Refs 5, 6 and 19) and heterogeneous media (e.g. Refs 9 and 22). Besides elucidating some of the various seismically-induced phenomena observed at ground surface, these types of studies have practical applications such as estimation of modified free field motions for soil–structure interaction,[18] construction of site-dependent response spectra for earthquake resistant design,[26] etc.

In order to model randomness in local site effects, a conceptually simple but computationally intense statistical simulation of ground motions induced by seismicity can be accomplished through use of conventional Monte Carlo simulations.[27] Newer, improved Monte Carlo simulations involving up to three spatial coordinates and capable of representing medium anisotropy through the use of spatial coherency functions can be found in the work of Ramadan and Novak.[28] Alternatively, it is possible to trace the filtering of the power spectral density function of ground motions through topsoil by modelling the upper soil layers as filters. For a linear system under random loading with conventional distributions (such as Gaussian), the methodologies developed for the corresponding deterministic problem can easily be recycled, especially if stationary conditions can be assumed and if the problem is solved in the frequency domain. Since the structure of geological media is extremely complicated and imprecisely known, unless very detailed physical measurements are carried out, an attractive alternative to sophisticated deterministic analyses is to introduce stochasticity by considering soil to have random material properties and/or random layer geometry. A detailed review on the representation of the ground as a stochastic medium with emphasis on seismically induced motions can be found in Manolis.[29] As far as modelling of uncertainties in the material properties and layer geometry of the local site is concerned, the perturbation approach is widely used in conjunction with appropriate analytical or numerical techniques originally developed for deterministic analyses. For instance, Kiyono *et al.*[30] employ the discrete wave number technique originally introduced by Aki and Larner[31] with perturbations for evaluating the seismic response of layered soil strata with irregular interfaces that fluctuate stochastically. Examples focus on sites with two or three layers of random thickness and of periodic structure in the horizontal direction, while the results are in the form of means and variances for the individual layer transfer functions.

Most numerical work, however, employs the finite element method. More conventional approaches follow Taylor series expansions of the random states about the deterministic one, as originally outlined in structural mechanics by Vanmarke *et al.* [32] and Liu *et al.*[33] As examples we cite Refs 34 and 35 which employ the probabilistic finite element method to examine layered soil with random density, damping and wave speed as well as a strain-dependent shear modulus under stochastic input represented by the Kanai–Tajimi filter. In the former reference, the mean and variance of the shear strain is obtained through a Taylor series expansion of the system matrices in the frequency domain. Also, wave propagation through layered soil with random

properties is examined in Ref. 36 by a Taylor series expansion of the complex frequency response function of each layer, which is subsequently compared with Monte Carlo simulations. More novel finite element approaches are based on expansions in the spatial coordinate using stochastic functionals, such as the polynomial chaos expansions pioneered in Ghanem and Spanos.[37] As an example, we cite the use of such expansions in conjunction with a Fourier transform with respect to time to model layered soil with stochastic properties and resting on bedrock.[38] In general, the efficient solution of meaningful engineering problems regarding local site effects and soil–structure interaction phenomena necessitates the use of coupled finite element-boundary element techniques.[39] A necessary ingredient for the latter method is the existence of appropriate fundamental solutions that are capable of representing both radiation and material damping effects so that only part of the far field that abuts the near field needs to be modelled. Furthermore, the introduction of material stochasticity in these numerical models[29] allows for an overall representation of the inevitable fluctuations in the structure of the geological medium that are difficult, if not impossible, to quantify.

In brief, the paper is structured as follows: at first, vector wave propagation in a three dimensional, continuously inhomogeneous medium is examined under the restriction of wave dependence in only one of the three orthogonal coordinates and for time-harmonic conditions. Subsequently, an algebraic transformation is applied to the uncoupled system of equations for the three displacement components and a solution is obtained subject to certain constraints on the variation of the elastic modulus and density profiles. These constraints yield quite general and realistic wavespeed profiles. Furthermore, the solution is cast in terms of a Green's function which includes the effect of a horizontal, traction-free surface. Since it is of interest to compare the continuously inhomogeneous medium with the more commonly used layered one, a discussion of the well-known transfer function approach for horizontal layers is included. Finally, perturbations are introduced for an efficient determination of Green's functions for wave propagation in viscoelastic heterogeneous media that exhibit small randomness in their material properties. Closed form solutions for the mean value and covariance of the wave speed profile and of the corresponding fundamental solutions are obtained that can be used within the context of boundary element formulations for wave scattering problems, as discussed in Refs such as 10 and 39. The examples focus on a comparison of the aforementioned models and the conditions under which similarities in the response between continuously heterogeneous and layered geological media are observed are discussed. Finally, numerical results are obtained for stochastic wave propagation through heterogeneous ground which are then compared with Monte Carlo simulations.

## GOVERNING EQUATIONS

The equations governing elastic waves in a heterogeneous medium [see Fig. 1(a)] are (e.g. Aki and Richards[2]),

$$\rho u_{x,tt} = [\lambda e + 2\mu u_{x,x}]_{,x} + [\mu(u_{x,y} + u_{y,x})]_{,y} + [\mu(u_{x,z} + u_{z,x})]_{,z} \tag{1a}$$

$$\rho u_{y,tt} = [\lambda e + 2\mu u_{y,y}]_{,y} + [\mu(u_{y,z} + u_{z,y})]_{,z} + [\mu(u_{y,x} + u_{x,y})]_{,x} \tag{1b}$$

$$\rho u_{z,tt} = [\lambda e + 2\mu u_{z,z}]_{,z} + [\mu(u_{z,x} + u_{x,z})]_{,x} + [\mu(u_{z,y} + u_{y,z})]_{,y} \tag{1c}$$

where the dilatation, $e$, is $u_{x,x} + u_{y,y} + u_{z,z}$ and there are no body forces. For time harmonic waves, of the form $\exp[-i\omega t]$, where $\omega = 2\pi f$ is the frequency in rad/s, in a layered medium, i.e. one in which the material parameters vary only in one direction (taken to be the $x$ direction here for convenience in the mathematical manipulations rather than the usual physically based choice of the $z$ direction), these equations reduce to

$$-\rho\omega^2 u_x = [\lambda e + 2\mu u_{x,x}]_{,x} + \mu(u_{x,y} + u_{y,x})_{,y} + \mu(u_{x,z} + u_{z,x})_{,z} \tag{2a}$$

$$-\rho\omega^2 u_y = \lambda e_{,y} + 2\mu u_{y,yy} + \mu(u_{y,z} + u_{z,y})_{,z} + [\mu(u_{y,x} + u_{x,y})]_{,x} \tag{2b}$$

$$-\rho\omega^2 u_z = \lambda e_{,z} + 2\mu u_{z,zz} + [\mu(u_{z,x} + u_{x,z})]_{,x} + \mu(u_{z,y} + u_{y,z})_{,y} \tag{2c}$$

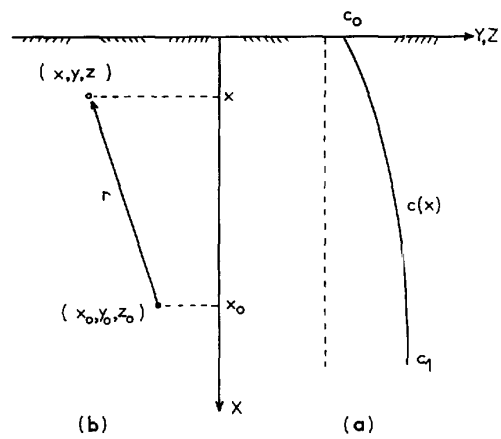


**Fig. 1.** (a) Depth variation of shear wave speed $c(z)$ in a continuously heterogeneous medium; (b) typical source–receiver configuration.

## ONE DIMENSIONAL WAVES

For waves with only an $x$ dependence, these equations further reduce to

$$-\rho\omega^2 u_x = [(\lambda + 2\mu)u_{x,x}]_{,x} \tag{3a}$$

$$-\rho\omega^2 u_y = [\mu u_{y,x}]_{,x} \tag{3b}$$

$$-\rho\omega^2 u_z = [\mu u_{z,x}]_{,x} \tag{3c}$$

These form an uncoupled system of equations on $u_x$, $u_y$ and $u_z$ of the form discussed by Shaw and Makris[40] for an analogous acoustic problem reduced to one dimension,

$$\mathrm{d}[K_i(x)\,\mathrm{d}u_i(x)/\mathrm{d}x]/\mathrm{d}x + N_i(x)u_i(x) = 0 \tag{4}$$

where $u_1$, $u_2$ and $u_3$ are $u_x$, $u_y$ and $u_z$, respectively, and $K_1$ is $(\lambda + 2\mu)$ and $K_2 = K_3 = \mu$ with $N$ equal to $\rho\omega^2$ in all these cases.

A transformation, $T_i = K_i^{1/2}u_i$ (no summation implied) leads to

$$K_i^{1/2}\{\mathrm{d}^2T_i/\mathrm{d}x^2 + [(\mathrm{d}K_i/\mathrm{d}x)^2/(4K_i^2) - (\mathrm{d}^2K_i/\mathrm{d}x^2)/(2K_i) + (N/K_i)]T_i\} = 0 \tag{5}$$

If the coefficient of the second term is a constant, $\beta_i^2$, i.e.

$$[(\mathrm{d}K_i/\mathrm{d}x)^2/(4K_i^2) - (\mathrm{d}^2K_i/\mathrm{d}x^2)/(2K_i) + (N/K_i)] = \beta_i^2 \tag{6}$$

and $N(x)$ is related to $K_i(x)$, or more conveniently, to $W_i = K_i^{1/2}$, through

$$N(x) = A_i(x)W_i + B_iW_i^2 \tag{7}$$

the material relationship between density and the Lamé parameters would be defined by

$$\mathrm{d}^2W_i/\mathrm{d}x^2 + (\beta_i^2 - B_i)W_i = A_i(x) \tag{8}$$

where $B_i$ is a set of arbitrary constants and $A_i(x)$ is a set of arbitrary functions, chosen so that this equation may be easily solved for $W_i(x)$. Then the equation in $T_i(x)$ is

$$\mathrm{d}^2T_i(x)/\mathrm{d}x^2 + \beta_i^2T_i(x) = 0 \tag{9}$$

whose solution is, for real $\beta_i^2$,

$$T_i(x) = c_i^{(1)}\exp[\mathrm{i}\beta_i x] + c_i^{(2)}\exp[-\mathrm{i}\beta_i x] \tag{10}$$

representing waves in the $\pm x$ direction. Note that displacements and strains travel with constant phase speed $\beta$. Since the original displacements are $u_i = K_i^{-1/2}T_i$, this provides a position dependent wave amplitude, i.e.

$$u_i(x) = K_i^{-1/2}(x)\{c_i^{(1)}\exp[\mathrm{i}\beta_i x] + c_i^{(2)}\exp[-\mathrm{i}\beta_i x]\} \tag{11}$$

The actual material variation is found by fitting observations to solve eqn (8) for $W_i$ and eqn (7) for $N$, essentially simultaneously. Some examples of the acoustic case, i.e. one dependent variable, are given in Shaw and Makris,[40] for such forms as

$$A_i(x) = \alpha_i^{(0)} + \beta_i^{(0)}x + \sum_{j=1}^{M}(\alpha_i)^{(j)}\exp(-(\gamma_i)_j x) \tag{12}$$

leading to forms for $W_i(x)$ such as

$$W_i(x) = -(\alpha_i^{(0)} + \beta_i^{(0)}x)/\lambda_i^2 + \sum_{j=1}^{M}(\alpha_i)^{(j)}\exp(-(\gamma_i)_j x)/((\gamma_i)_j^2 - \lambda_i^2) + a_i^{(1)}\exp(\lambda_i x) + a_i^{(2)}\exp(-\lambda_i x) \tag{13}$$

with $\lambda_i^2 = B_i - \beta_i^2$ and with eqn (7) defining $N$ in terms of $W_i$.

The dilatation, $e$, is simply $u_{x,x}$, while the mathematical rotations are $\omega_z = u_{y,x}$ and $\omega_y = -u_{z,x}$. They are then found as

$$e = \frac{\mathrm{d}}{\mathrm{d}x}\{W_1(x)[c_1^{(1)}\exp[\mathrm{i}\beta_1 x] + c_1^{(2)}\exp[-\mathrm{i}\beta_1 x]\} \tag{14}$$

$$\omega_z = \frac{\mathrm{d}}{\mathrm{d}x}\{W_2(x)[c_2^{(1)}\exp[\mathrm{i}\beta_2 x] + c_2^{(2)}\exp[-\mathrm{i}\beta_2 x]\} \tag{15}$$

$$\omega_y = -\frac{\mathrm{d}}{\mathrm{d}x}\{W_3(x)[c_3^{(1)}\exp[\mathrm{i}\beta_3 x] + c_3^{(2)}\exp[-\mathrm{i}\beta_3 x]\} \tag{16}$$

These still have the form of propagating waves but with position dependent amplitudes and modified wavenumbers.

Although this may seem to be an 'inverse' approach, the form of eqns (14–16) allows for quite general solutions for $W_i$ and thus $N$ as well. While this is a very restricted solution in that it represents waves propagating in only one direction, that of the layering, it is of interest in such activities as seismic prospecting, although such uses generally involve transient waves for which this formulation would be a Fourier transformed form.

## FUNDAMENTAL SOLUTION

In order to obtain a fundamental solution (Green's function) for the problem described in the previous section, eqn (4) will be solved for a point source in the infinite continuum. As discussed in Shaw *et al.*[10,40], the forcing function is of the form

$$Q(x, x_0) = Q_0\delta(x - x_0) \tag{17}$$

and acts at source $x_0$ with magnitude $Q_0$. Point $x$ is the receiver and a typical source–receiver configuration is shown in Fig. 1(b). As a result, eqn (9) now reads as

$$\nabla^2T(x) + \beta^2T(x) = -K^{-1/2}(x)Q_0\delta(x - x_0) \tag{18}$$

where $T(x)$ and $\beta$ are respectively identified with $T_3(x)$ and $\beta_3$, while $\nabla^2$ is the Laplacian. Thus, we are considering horizontally polarized shear (SH) wave propagation in the continuum with

$$c^2(x) = \mu(x)/\rho(x) = \omega^2 K_3(x)/N(x) \tag{19}$$

as the position-dependent, local wave speed. Based on the translational properties of the Dirac delta function $\delta$, the right-hand side of eqn (18) can be written as $-K^{-1/2}(x_0)Q_0\delta(x-x_0)$. By replacing transformation $T(x)$, eqn (18) becomes

$$\begin{aligned}\nabla^2\{K^{1/2}(x)U(x,x_0)K^{1/2}(x_0)\}\\ + \beta^2\{K^{1/2}(x)U(x,x_0)K^{1/2}(x_0)\}\\ = -Q_0\delta(x-x_0)\end{aligned} \tag{20}$$

where displacement $U(x,x_0)$ can be viewed as the out-of-plane component $u_z$ of eqn (3c) with both source and receiver restricted to lie along the $x$-axis. The bracketed expression in the above equation is identified upon inspection with the Green's function $G_h(r)$, $r = |(x-x_0)|$, for the standard one-dimensional Helmholtz equation.[41] Thus,

$$G_h(r) = Q_0 \exp(\mathrm{i}\beta r)/(2\mathrm{i}\beta) \tag{21}$$

by ignoring the ingoing wave contribution. Therefore,

$$U(r) = Q_0 K^{-1/2}(x)K^{-1/2}(x_0)\exp(\mathrm{i}\beta r)/(2\mathrm{i}\beta) \tag{22}$$

where $r$ is the radial distance between source and receiver, while $x_0$ and $x$ respectively are their depth coordinates. Equation (22) is the exact fundamental solution of the heterogeneous Helmholtz equation [see also eqn (10)] provided the constraint dictated by eqn (6) is satisfied. Finally, in order to restore the appropriate dimensionality back to the fundamental solution, $U(r)$ must be multiplied by the reference stiffness $K$ at infinite depth (or at the bottom of a layer) where a homogeneous state is assumed to exist, i.e.

$$G(r) = K(x \to \infty)U(r) = G_h(r)K_\infty/(W(x)W(x_0)) \tag{23}$$

where $G$ is now the Green's function for the heterogeneous medium.

Viscoelastic material behavior can be introduced in the above fundamental solution through a complex number representation of the shear modulus $\mu$.[42] For the simple (yet realistic) case of Kelvin's solid we have that

$$\mu_\mathrm{v} = q_0 + \mathrm{i}\omega q_1 \tag{24}$$

where $q_0$ and $q_1$ are model parameters. The corresponding wave number is

$$\beta^2 = \omega^2/c_\mathrm{v}^2 = \omega^2\rho/\mu_\mathrm{v} \tag{25}$$

with real and imaginary parts given as

$$\begin{aligned} Re\{\beta\} &= \omega\sqrt{\rho/q_0}\\ Im\{\beta\} &= \mathrm{Re}\{\beta\}\sqrt{\omega q_1/q_0}\end{aligned} \tag{26}$$

The above equation indicates that $q_0$ is the average real shear modulus $\mu$ of the medium. Furthermore, $q_1$ can be computed[22] through the relation

$$\delta = 2\pi\sqrt{\omega q_1/q_0} \tag{27}$$

where $\delta$ is the logarithmic decrement of cyclic motions in a free-vibration environment. We finally note that $\delta = \pi/Q$, where quality factor $Q$ measures overall energy loss per cycle of vibration due to material damping.[3] Although the introduction of viscoelasticity appears to be a somewhat *ad-hoc* procedure, it is consistent with the present model and merely requires the coefficients appearing in eqn (13) to be complex quantities.

## MATERIAL PARAMETER PROFILES

We now return to eqns (7) and (13) (without subscript $i$) in order to recover realistic density, shear modulus and shear wave speed profiles for a stratified medium. Without loss of generality, we reformulate the aforementioned equations due to the presence of a complex, frequency dependent wavenumber $\beta(\omega)$ and retain a limited number of terms,[22] i.e.

$$\begin{aligned} W(x,\omega) &= \alpha_0/\beta^2 + \alpha_1\exp(-\gamma x)/(\gamma^2+\beta^2)\\ &\quad + \alpha_2\exp(\mathrm{i}\beta x) + \alpha_3\exp(-\mathrm{i}\beta x)\\ N(x,\omega) &= A(x)W(x,\omega)\\ &= \{\alpha_0 + \alpha_1\exp(-\gamma x)\}W(x,\omega)\end{aligned} \tag{28}$$

and

$$c(x,\omega) = \omega W(x,\omega)/\sqrt{N(x,\omega)} \tag{29}$$

For problems where the depth coordinate increases ($x > 0$), the $\alpha_3$ term in eqn (28) must be suppressed because it leads to incoming waves.

Boundary conditions for material parameters $W$ and $N$ are prescribed at the horizontal surface $x = 0$ and at depth $x = L$. The resulting set of equations for determining constants $\alpha_0$, $\alpha_1$, $\alpha_2$ and wavenumber $\beta$ are

$$\begin{aligned} W(x=0) &= W_0 = \alpha_0/\beta^2 + \alpha_1/(\gamma^2+\beta^2) + \alpha_2\\ N(x=0) &= N_0 = \{\alpha_0+\alpha_1\}W_0\\ W(x=L) &= W_1 = \alpha_0/\beta^2 + \alpha_1\exp(-\gamma L)/(\gamma^2+\beta^2)\\ &\quad + \alpha_2\exp(\mathrm{i}\beta L)\\ N(x=L) &= N_1 = \{\alpha_0 + \alpha_1\exp(-\gamma L)\}W_1\end{aligned} \tag{30}$$

A rather elegant solution results if the inhomogeneous stratum depth $L$ is large compared to the wavelength.[22] In that case, terms $\exp(-\gamma L)$ and $\exp(\mathrm{i}\beta L)$ can be

ignored. We therefore have

$$\begin{aligned} \alpha_0 &= \beta_1^2 W_1 \\ \alpha_1 &= \beta_0^2 W_0 - \beta_1^2 W_1 \\ \alpha_2 &= W_0 - W_1 - \alpha_1/(\gamma^2 + \beta^2) \\ \beta &= \beta_1 \end{aligned} \tag{31}$$

with $\beta_0$ and $\beta_1$ defined as wavenumbers that correspond to the top and bottom of the inhomogeneous stratum, i.e.

$$\beta_0 = \omega/c_0 \quad \text{and} \quad \beta_1 = \omega/c_1 \tag{32}$$

There are insufficient conditions for determining parameter $\gamma$, but parametric studies[22] have shown that values in the neighborhood of 0·1 produce realistic wavespeed profiles for a wide range of inhomogeneous soil deposits. Furthermore, $\gamma$ will be converted into a random parameter in the discussion on media with stochastic material parameters.

It should be noted at this point that the last part of eqn (31) implies a wavenumber which depends solely on values of the material parameters measured at large depth, where the material is assumed to attain a homogeneous structure. Furthermore, only the shear modulus $\mu = K = W^2$ is a complex quantity, while density $\rho = N/\omega^2$ must remain real for physical reasons. By substituting all previous results in eqns (28), we recover a complete solution for the material parameters as

$$\begin{aligned} W(x,\omega) = {} & W_1 + (\beta_0^2 W_0 - \beta^2 W_1)\exp(-\gamma x)/(\gamma^2 + \beta^2) \\ & + \{W_0 - W_1 - (\beta_0^2 W_0 - \beta^2 W_1)/(\gamma^2 + \beta^2)\} \\ & \times \exp(\mathrm{i}\beta x) \\ N(x,\omega) = {} & \{\beta^2 W_1 + (\beta_0^2 W_0 - \beta^2 W_1) \\ & \times \exp(-\gamma x)\} W(x,\omega) \end{aligned} \tag{33}$$

From the above, the local wavespeed profile $c(x)$ is determined through eqn (29) and the corresponding Green's function is synthesized as indicated by eqns (22) and (23).

## METHOD OF IMAGES

The unidimensional wave propagation situation described in the previous sections results in a stress field with only one non-zero component, namely

$$\sigma_{xz} = \mu \partial u_z/\partial x \tag{34}$$

In the presence of a horizontal, traction-free surface at $x = 0$ as shown in Fig. 1(b), stress component $\sigma_{xz}$ must vanish. This boundary condition is realized through introduction of an image source reflected across the horizontal plane, i.e. at $x = -x_0$. Thus, the augmented Green's function is

$$G^*(r, r', \omega) = G(r, \omega) + G(r', \omega) \tag{35}$$

where $r = |x - x_0|$ and $r' = |x + x_0|$. Substitution of $G^*(r, r', \omega)$ into eqn (34) yields

$$\sigma_{xz} = \mu\left[\frac{\partial G(r,\omega)}{\partial r}\frac{\partial r}{\partial x} + \frac{\partial G(r',\omega)}{\partial r'}\frac{\partial r'}{\partial x}\right] \tag{36}$$

For receivers placed directly on the traction-free surface, we have that $r = r'$ and consequently

$$\frac{\partial r}{\partial x} = \frac{-x_0}{r}, \qquad \frac{\partial r'}{\partial x} = \frac{x_0}{r} \tag{37}$$

Thus, the correct boundary conditions are realized as

$$\sigma_{xz} = 0 \tag{38}$$

irrespective of the particular form of $G(r, \omega)$.

## WAVE PROPAGATION THROUGH HORIZONTAL LAYERS

The ensuing discussion is based on Safak's[8,43] work, who introduced some improvements in the frequency domain method of Haskell[5] for studying site amplification in layered media by using the discrete time wave propagation technique. Consider first a soil layer with density $\rho_s$ and shear wave speed $c_s$ resting on rock with corresponding material properties $\rho_r$ and $c_r$, as shown in Fig. 2(a). The reflection coefficient is defined as

$$R = (\rho_r c_r - \rho_s c_s)/(\rho_r c_r + \rho_s c_s) \tag{39}$$

while $t = \tau$ is the one-way travel time for the SH wave emanating from rock to reach the top of the overlying soil deposit. Material damping due to internal friction in the soil is introduced through the quality factor $Q$,

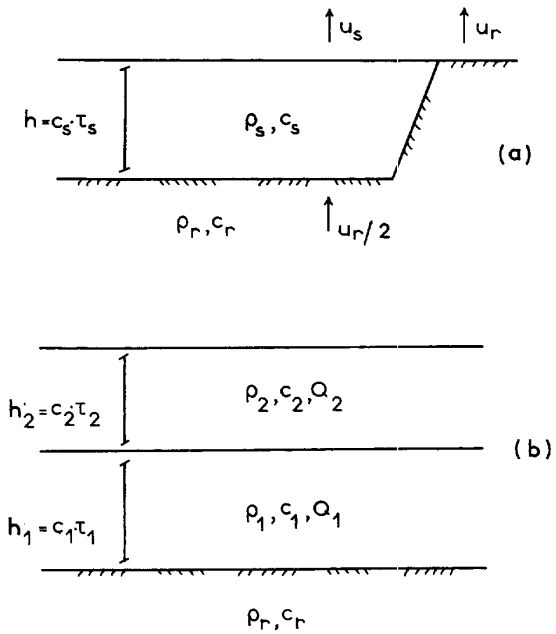


**Fig. 2.** Layered medium comprising of (a) one and (b) two soil layers resting on rock.

which measures energy loss per cycle of motion. As previously mentioned, $1/Q$ is known as the dissipation constant and is equal to $2\,Im(c_s)/Re(c_s)$ in a complex representation of the wave speed $c_s$, while ratio $\pi/Q$ is equivalent to the logarithmic decrement $\delta$ of viscously damped free vibrations. The solution methodology is cast in the time domain by defining the usual transmitted and reflected waves. Furthermore, attenuation in the transfer function representing wave amplitude reduction is handled through the introduction of a low-pass filter with sampling time interval $t = T$. The Fourier transform of this transfer function is

$$\begin{aligned} H_2(f) &= U_s(f)/U_r(f) \\ &= \{(1 + R - i/4Q)\exp(-i2\pi f\tau(1 - i/2Q))\} \\ &\quad \div \{1 + (R - i/4Q)\exp(-i4\pi f\tau(1 - i/2Q))\} \end{aligned} \tag{40}$$

where $U_s(f)$ and $U_r(f)$ respectively are the Fourier transforms of the ground motions $u_s(t)$ and $u_r(t)$ recorded at the soil free surface and at rock outcrop. In the above, $f$ is the frequency in Hertz. Finally, approximate values for the layer eigenfrequencies $f_k$ as $1/4Q \to 0$ are

$$f_k = k/4\tau, \qquad k = 1, 3, 5 \tag{41}$$

while the maximum amplification recorded at first eigenfrequency is

$$|H_2(f)|_{\max} = (1 + R)/(1 - R) \tag{42}$$

Next, Safak[8] extends his approach to the multilayered ($j = m, m-1, \ldots, 2, 1$) case, where $j = m$ is the top layer and the first ($j = 1$) layer rests on bedrock, by employing matrix formalism. It is possible to get a rather simple expression for the dimensionless transfer function $H_3(f)$ of the two layer site [see Fig. 2(b)] as

$$\begin{aligned} H_3(f) &= \{\lambda_1\lambda_2(1+R_1)(1+R_2)\exp(-i2\pi f(\tau_1+\tau_2))\} \\ &\quad \div \{(1 + \lambda_1^2 R_1 \exp(-i4\pi f\tau_1) \\ &\quad + \lambda_2^2 R_1 R_2 + \exp(-i4\pi f\tau_2)) \\ &\quad + \lambda_1^2\lambda_2^2 R_2 \exp(-i4\pi f(\tau_1+\tau_2))\} \end{aligned} \tag{43}$$

where the damping parameters $\lambda_j$ ($j = 1, 2$) are defined as

$$\lambda_j = 0{\cdot}5(1 - \alpha_j)(1 + q^{-1})/(1 - \alpha_j q^{-1}) \tag{44}$$

with

$$\begin{aligned} \alpha_j &= (1 - \sin\theta_j)/\cos\theta_j \\ \theta_j &= (\ln 2)Q_j T/\tau_j \le \pi \\ q &= \exp(i2\pi f T) \end{aligned} \tag{45}$$

Furthermore, all symbols appearing in the above expression have been defined in conjunction with the single layer case. The above results will be used in the numerical examples section as a means of comparing unidimensional shear wave propagation in continuously inhomogeneous versus horizontally layered media.

## PERTURBATION APPROACH

An efficient technique for handling medium stochasticity is through use of the perturbation approach.[10] Despite its efficiency, however, the perturbation method has several drawbacks: it is valid for small variabilities, divergent (or secular) terms appear in the expansions, and it is often necessary to compute higher statistical moments in order to get a more detailed solution that is valid for larger variabilities. Furthermore, this last goal conflicts with the previous one, i.e. higher moments contain secular terms that diverge faster than those appearing in the lower order moments. There are ways of combating divergence in the perturbation approach, i.e. through the imposition of orthogonality conditions or through the use of the Fourier transformation. First order perturbations, however, remain a valuable analysis tool due to their simplicity. In our case, it will be recalled that the expressions for the wave speed profile $c(x)$ and the Green's function $G(r)$ contained a parameter $\gamma$ that is now considered to be a member of random set $\Gamma$, i.e.

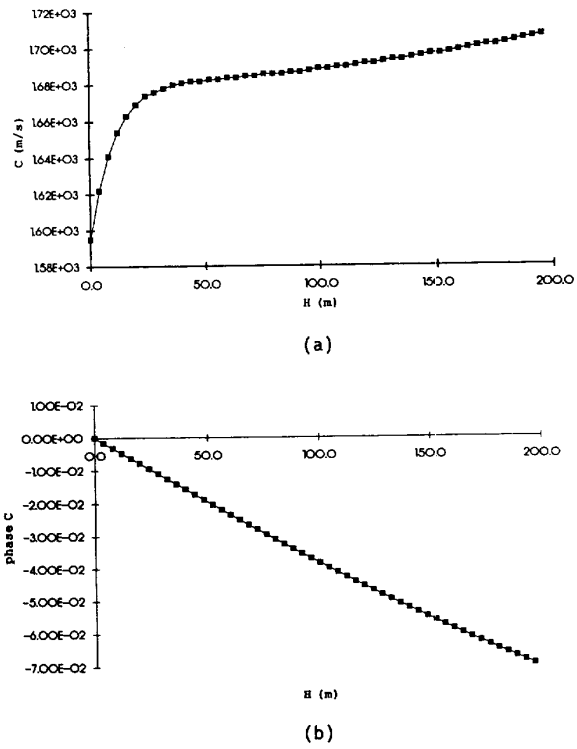


**Fig. 3.** Shear wave speed (a) amplitude and (b) phase angle variation with depth at $f = 1$ Hz.

$$\gamma = \gamma_m + \varepsilon\gamma_f \tag{46}$$

where $\gamma_m$ is the mean value, $\gamma_f$ is a zero-mean fluctuation and $\varepsilon$ is a small number. By introducing the expectation operator $E$, which denotes statistical averaging, we have that $E(\gamma) = \langle\gamma\rangle = \gamma_m$ is the mean and that $\langle(\gamma - \gamma_m)^2\rangle = \langle(\gamma_f^2)\rangle = \sigma_\gamma^2$ is the standard deviation of this random parameter. It is not necessary in a first order perturbation to assume any particular distribution for the random parameter at hand.

In view of the structure of the random parameter $\gamma$, it is assumed that all quantities of interest, including the material properties $W(x,\gamma)$, $N(x,\gamma)$ and $c(x,\gamma)$ as well as the Green's function $G(r,\gamma)$, can be written in terms of a mean value (subscript m) plus a fluctuation (subscript f), i.e.,

$$W(x,\gamma) = W_m(x) + \varepsilon W_f(x,\gamma) \tag{47}$$

etc. In all cases, the mean value is the deterministic solution given in the previous sections and can be recovered by replacing $\gamma$ by its mean value $\gamma_m$. This is a consequence of the first order perturbation technique since, in general, the mean value of a stochastic process is not equal to the equivalent deterministic solution obtained for the mean value of the dependent random variable. The fluctuations are obtained by substituting eqn (46) in the relevant expressions for the material properties, carrying out the expansions for small $\varepsilon$, and then equating powers of $\varepsilon$. The mean value is recovered and the fluctuation has a zero value about the mean due to linearization inherent in small argument expansions. Before proceeding with the infinite layer solution, the following small argument expansions must be given:

$$\begin{aligned} \gamma^2 &\approx \gamma_m^2 + \varepsilon 2\gamma_m\gamma_f \\ e^{-\gamma x} &\approx e^{-\gamma_m x} - \varepsilon\gamma_f x e^{-\gamma_m x} \end{aligned} \tag{48}$$

In the above, $\gamma$ has units of 1/length. We first note here that both local wave speed profile and the Green's function are stochastic processes and not random fields since they depend, in addition to $\gamma$, on one spatial variable. The appearance of secular terms of the type $x\exp(-\gamma x)$ in the above expansions must also be noted. These terms are, however, under the control of the exponential decay factor and do not present a problem since $\gamma_m x > 1{\cdot}0$.

## Infinite layer solution

In the infinite layer solution, constants $\alpha_0$, $\alpha_1$ and the wavenumber $\beta$ remain deterministic and thus have no fluctuating components. Using the perturbation approach, we recover the mean values $\alpha_0^m$, $\alpha_1^m$, $\alpha_2^m$ and $\beta_m$ that appear in eqn (31) for $\gamma = \gamma_m$, while the

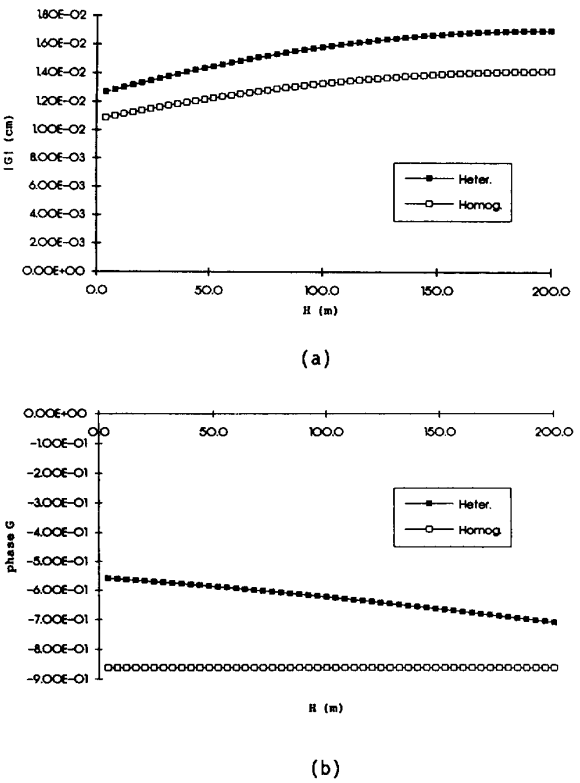


**Fig. 4.** Green's function (a) amplitude and (b) phase angle variation with depth at $f = 1$ Hz, with $c_{top} = 0{\cdot}9c$.

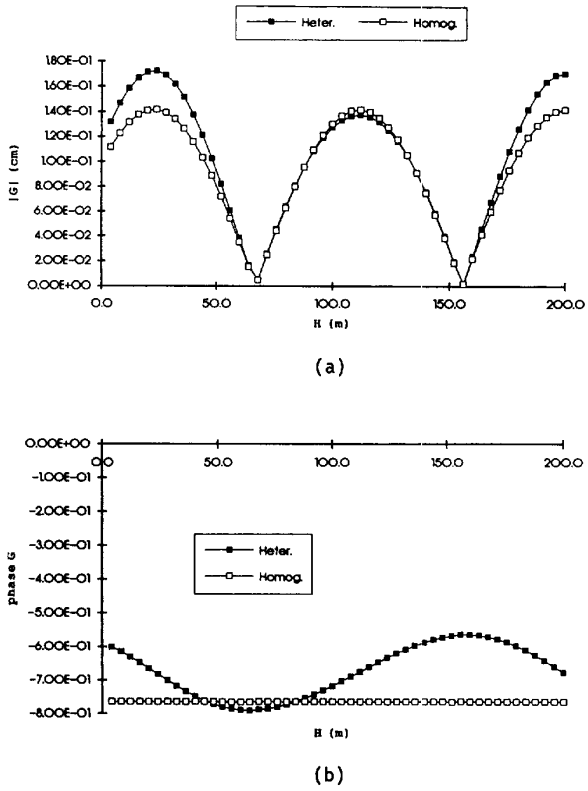


**Fig. 5.** Green's function (a) amplitude and (b) phase angle variation with depth at $f = 10$ Hz, with $c_{top} = 0{\cdot}9c$.

fluctuation is as follows:

$$\alpha_2^{\mathrm{f}} = \gamma_{\mathrm{f}}\tilde{\alpha}_2^{\mathrm{f}} = 2\gamma_{\mathrm{m}}\gamma_{\mathrm{f}}\alpha_1^{\mathrm{m}}/(\beta_{\mathrm{m}}^2 + \gamma_{\mathrm{m}}^2)^2 \tag{49}$$

Given the above fluctuation, application of the perturbation method to the material parameters of the problem respectively yields the fluctuations of the elastic modulus and of the local wave speed as

$$W_{\mathrm{f}}(x,\gamma) = \gamma_{\mathrm{f}}\tilde{W}_{\mathrm{f}}(x) \tag{50}$$

with

$$\tilde{W}_{\mathrm{f}}(x) = [\mathrm{e}^{-\gamma_{\mathrm{m}}x}\{-\alpha_1^{\mathrm{m}}(x + 2\gamma_{\mathrm{m}}/(\beta_{\mathrm{m}}^2 + \gamma_{\mathrm{m}}^2))\} + \tilde{\alpha}_2^{\mathrm{f}}\,\mathrm{e}^{\mathrm{i}\beta_{\mathrm{m}}x}(\beta_{\mathrm{m}}^2 + \gamma_{\mathrm{m}}^2)]/(\beta_{\mathrm{m}}^2 + \gamma_{\mathrm{m}}^2) \tag{51}$$

and

$$c_{\mathrm{f}}^2(x,\gamma) = \gamma_{\mathrm{f}}\omega^2\tilde{c}_{\mathrm{f}}^2(x) \tag{52}$$

with

$$\tilde{c}_{\mathrm{f}}^2(x) = [\tilde{W}_{\mathrm{f}}(x) - W_{\mathrm{m}}(x) \times \{\mathrm{e}^{-\gamma_{\mathrm{m}}x}(-\alpha_1^{\mathrm{m}}x)\}/(\alpha_0^{\mathrm{m}} + \alpha_1^{\mathrm{m}}\,\mathrm{e}^{-\gamma_{\mathrm{m}}x})] \div (\alpha_0^{\mathrm{m}} + \alpha_1^{\mathrm{m}}\,\mathrm{e}^{-\gamma_{\mathrm{m}}x}) \tag{53}$$

As before, the mean values $W_{\mathrm{m}}(x)$ and $c_{\mathrm{m}}(x)$ are the deterministic values given by eqns (28) and (29) with $\gamma$ replaced by $\gamma_{\mathrm{m}}$.

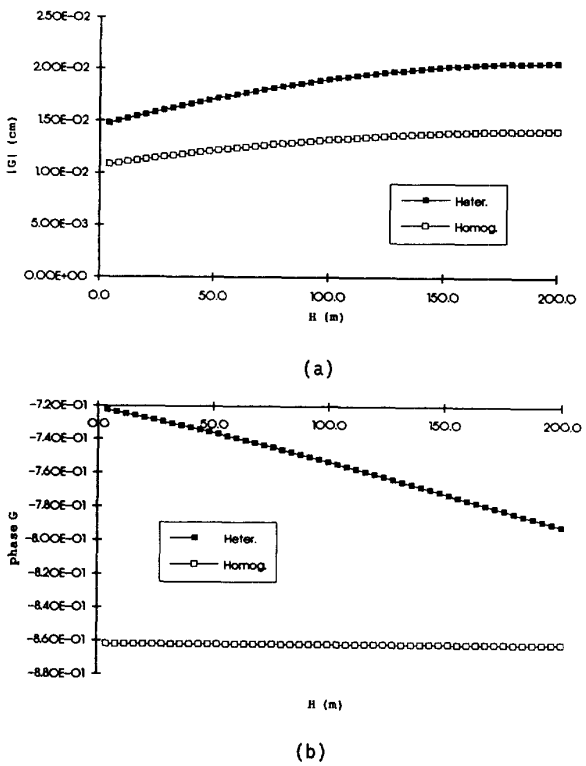


**Fig. 6.** Green's function (a) amplitude and (b) phase angle variation with depth at $f = 1$ Hz, with $c_{\mathrm{top}} = 0{\cdot}8c$.

Finally, the above development can now be used in conjunction with the Green's function, which is also expressed as

$$G(r,\gamma) = G_{\mathrm{m}}(r) + \varepsilon G_{\mathrm{f}}(r,\gamma) \tag{54}$$

where the mean value $m_{\mathrm{G}}(r) = G_{\mathrm{m}}(r)$ is given by eqn (23) with $\gamma$ replaced by $\gamma_{\mathrm{m}}$. Also, the fluctuation is

$$G_{\mathrm{f}}(r,\gamma) = -G_{\mathrm{h}}(r)\{W_{\mathrm{m}}(x)W_{\mathrm{f}}(x_0,\gamma) + W_{\mathrm{m}}(x_0)W_{\mathrm{f}}(x,\gamma)\}/\{W_{\mathrm{m}}(x)W_{\mathrm{m}}(x_0)\}^2 \tag{55}$$

where $x_0$ and $x$ are source and receiver depth coordinates, respectively.

## Covariance matrices

The covariance matrix for the local wave speed is defined as

$$c_{\mathrm{c}}^2(x_i,x_j) = \langle c_{\mathrm{f}}^2(x_i,\gamma)\,c_{\mathrm{f}}^2(x_j,\gamma)\rangle \tag{56}$$

where $x_i$ and $x_j$ are two different depth coordinates. In view of eqn (52), the above covariance matrix assumes

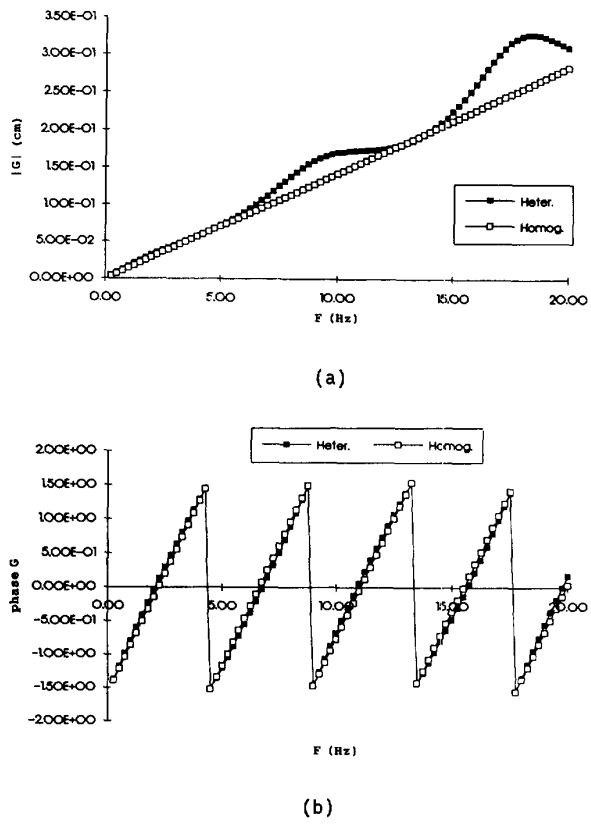


**Fig. 7.** Green's function (a) amplitude and (b) phase angle versus frequency for a 200 m layer with $c_{\mathrm{top}} = 0{\cdot}9c$.

the form

$$c_c^2(x_i, x_j) = \sigma_\gamma^2 \omega^4 \tilde{c}_f^2(x_i)\tilde{c}_f^2(x_j) \tag{57}$$

which is non-isotropic and explicitly depends on the standard deviation of $\gamma_f$.

Similarly, the covariance of the Green's function is defined as

$$c_g(r_i, r_j) = \langle G_f(r_i, \gamma) G_f(r_j, \gamma)\rangle \tag{58}$$

where $r_i$ and $r_j$ are two different receiver locations. The resulting expression is

$$\begin{aligned} c_g(r_i, r_j) = {} & G_h(r_i)G_h(r_j)\sigma_\gamma^2 \cdot \{W_m^2(x_0)\langle(\tilde{W}_f(x_i)(\tilde{W}_f(x_j)\rangle \\ & + W_m(x_0)W_m(x_i)\langle(\tilde{W}_f(x_0)(\tilde{W}_f(x_j)\rangle \\ & + W_m(x_0)W_m(x_j)\langle(\tilde{W}_f(x_0)(\tilde{W}_f(x_i)\rangle \\ & + W_m(x_i)W_m(x_j)\langle(\tilde{W}_f^2(x_0)\rangle\} \\ & \times [W_m(x_i)W_m(x_0)]^{-2}[W_m(x_j)W_m(x_0)]^{-2} \end{aligned} \tag{59}$$

where the individual covariances of $\tilde{W}_f(x)$ were discussed in conjunction with eqn (51). Also, $x_i$ and $x_j$ are the depth coordinates of radial distances $r_i$ and $r_j$ respectively. The covariance matrix for the Green's function is also non-isotropic and depends on the standard deviation of $\gamma_f$.

## NUMERICAL EXAMPLES

In this section we examine SH wave propagation through a stratified layer of sandstone 200 m deep under time-harmonic conditions. The following average material properties are assumed at large depth

$$\begin{aligned} \mu &= 5{\cdot}97 \times 10^9\,\text{Pa} \\ \rho &= 1900\,\text{kg/m}^3 \\ c &= 1770\,\text{m/s} \\ \delta &= 0{\cdot}1\,\text{dB} \end{aligned} \tag{60}$$

and, since we are examining seismic waves, the frequency range of interest is 0·02–20 Hz.

### Inhomogeneous medium

Sandstone is first modelled as a continuously inhomogeneous layer according to the methodology developed herein. The reference case assumes that the material properties given in eqn (60) apply at a depth greater than $x = 200$ m, past which the sandstone attains a nearly homogeneous structure, while the shear modulus at the horizontal surface ($x = 0$) is 81% of the value at large depth. Density remains constant, as does damping, so that the shear wave speed at the surface is 90% of

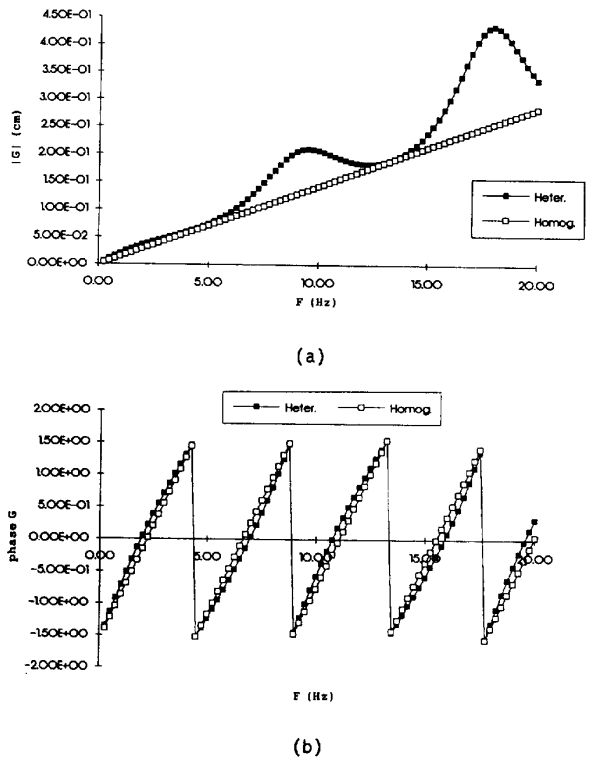


**Fig. 8.** Green's function (a) amplitude and (b) phase angle versus frequency for a 200 m layer with $c_{top} = 0{\cdot}8c$.

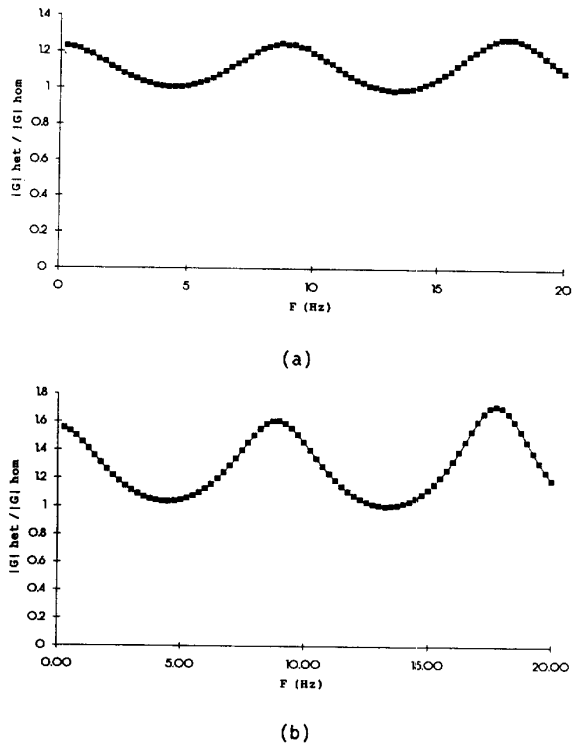


**Fig. 9.** Normalized Green's function amplitude versus frequency for a 200 m layer with (a) $c_{top} = 0{\cdot}9c$ and (b) $c_{top} = 0{\cdot}8c$.

the value at large layer depth. Since we assume visco-elastic material behavior, $c(x)$ is a complex number and Figs 3(a) and 3(b) respectively depict its amplitude and phase angle profiles with depth at a frequency $f = 1$ Hz according to eqns (29) and (33). The wave speed at the surface is therefore 1590 m/s, while at the bottom of the layer a value of 1710 m/s has been reached.

Using this particular profile, the Green's function given by eqns (23) and (35) is plotted versus radial distance $r = |x - x_0|$ in Figs 4 and 5 at frequencies of 1 and 10 Hz, respectively. The source–receiver configuration is the former at depth $x_0 = 200$ m, while the latter spans all the distance to top ($x = 0$) in 50 increments of 4 m. Since the Green's function is a complex quantity, the above figures plot both amplitude and phase angle. Concurrently shown is the Green's function of eqn (21), which corresponds to the equivalent homogeneous medium. Based on these plots, the following points can be made: (i) The displacement $u_z = G^*(r, \omega)$ amplitude due to a point source of unit magnitude is rather flat at low frequencies, while at higher frequencies it has a richer profile with nodes (roughly every third of the distance down) where the signal is nearly zero. The corresponding phase angle profile also becomes more varied as frequency increases; (ii) the presence of inhomogeneity in the form of continuously varying material parameters results in signal amplification of around 10% plus distortion in the phase angle. This is due to dispersion of the original signal as it travels through a medium whose wave speed changes continuously. More detailed studies[10,22] have shown that signal scattering becomes extremely intense in the absence of damping, but then with no distortion in the phase angle. We also note that the presence of the free surface results in a doubling of the signal's amplitude at that location. Furthermore, Fig. 6 plots the Green's function versus depth for the case where shear wave speed at surface is 80% of the value at large depths and for the reference frequency of 1 Hz. We observe that the result is higher scattering of the signal with amplification in the neighborhood of 30%, plus greater phase angle divergence.

Next we have a series of spectral plots (i.e. $G^*(r, \omega)$ versus $\omega$) in Figs 7 and 8 for $c(x = 0) = 0{\cdot}9c$ and $c(x = 0) = 0{\cdot}8c$, respectively. Also, the source is at $x = 200$ m while the receiver is at the surface. As before, we have both amplitude and phase angle plots. We observe that (i) the displacement amplitude varies

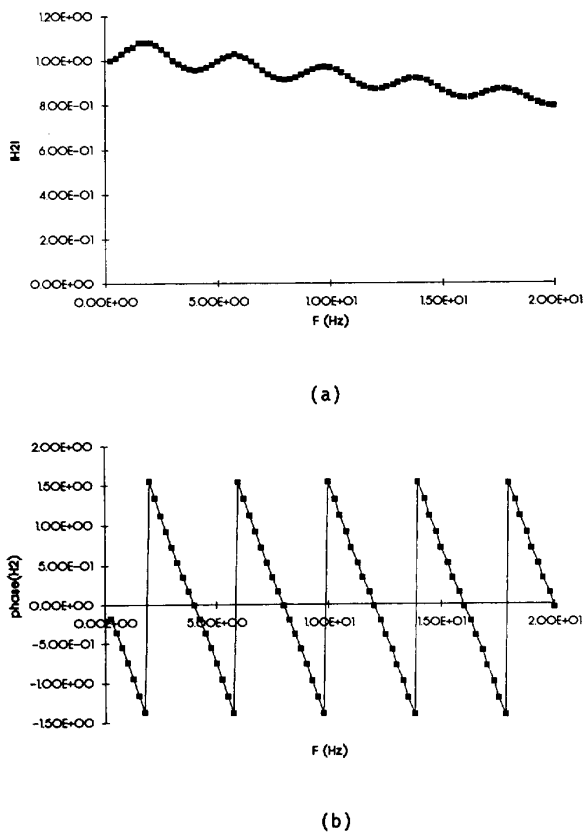


**Fig. 10.** Transfer function (a) amplitude and (b) phase angle for a two layered medium with $c_{top} = 0{\cdot}9c_{btm}$.

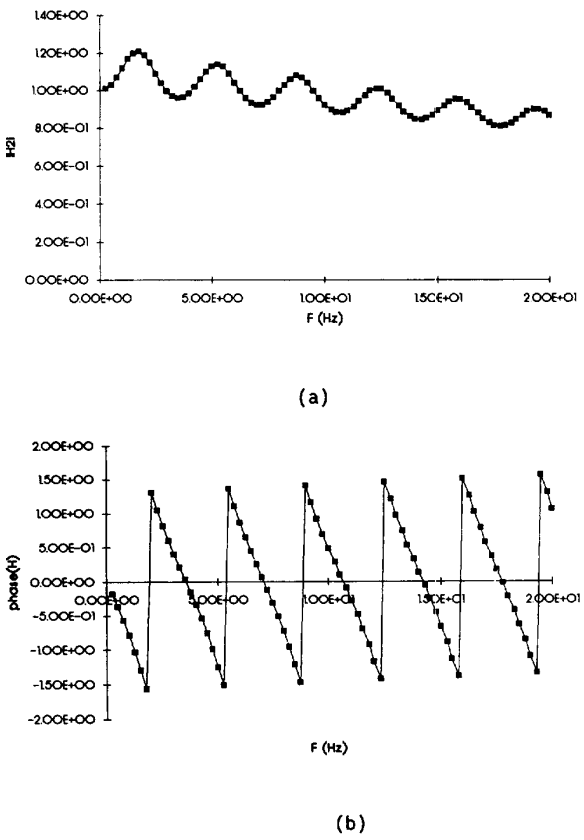


**Fig. 11.** Transfer function (a) amplitude and (b) phase angle for a two layered medium with $c_{top} = 0{\cdot}8c_{btm}$.

with frequency and this variation becomes more pronounced as the amount of inhomogeneity increases; (ii) the signal amplitude for the equivalent homogeneous case varies linearly, indicating that dispersion remains constant as a wave travels through a homogeneous viscoelastic layer; and (iii) there are rather minor changes in the phase angle as inhomogeneity is introduced. Finally, Fig. 9 plots the displacement amplitude for the inhomogeneous medium normalized by the amplitude corresponding to the homogeneous case (which is assumed to exist past a depth of $x = 200\,\mathrm{m}$) for both cases previously discussed. The important thing to notice is that the normalized signal's departure from a unit value becomes more pronounced with increasing medium heterogeneity.

**Layered medium**

We now adopt the more conventional representation of a geological medium such as soil in terms of horizontal layers.[5,8,19] At first, consider a sandstone layer with the material properties given by eqn (60) acting as 'bedrock' (subscript r) on which another sandstone layer (subscript s) of depth $h = 200\,\mathrm{m}$ rests [see Fig. 2(a)]. The only difference in material properties is that the top stratum has a shear wave speed $c = c_s = 0{\cdot}9c_r$. Figure 10 plots the transfer function $H_2(f)$ amplitude and phase angle corresponding to this case and given by eqn (40). Figures 11 and 12 are similar plots for $c_s = 0{\cdot}8c_r$ and $c_s = 0{\cdot}4c_r$, respectively. The relevant data needed in conjunction with eqn (40) are

$$\begin{aligned} R &= 0{\cdot}05 \qquad \tau = 0{\cdot}14\,\mathrm{s} \\ R &= 0{\cdot}11 \qquad \tau = 0{\cdot}13\,\mathrm{s} \\ R &= 0{\cdot}43 \qquad \tau = 0{\cdot}14\,\mathrm{s} \end{aligned} \tag{61}$$

for the aforementioned three cases, respectively, while $T = 0{\cdot}02$ and $Q = \pi/\delta = 31{\cdot}42$ for all. We observe that the transfer function amplitude becomes less smooth as the difference in layer to bedrock stiffness increases. The peaks in the amplitude plots correspond to layer eigenfrequencies and approximate values (whose accuracy is good for low values of damping $\delta$, i.e. high values of quality factor $Q$) are given by eqns (41) and (42). Thus, for a single layer representation we have eigenfrequencies that are about the same for all three cases ($f_k \simeq 1{\cdot}8, 5{\cdot}4, 8{\cdot}9, \ldots, \mathrm{Hz}$). Also, the first (maximum) amplitude peak at $f = f_1$ increases with increasing reflection coefficient $R$ and the values registered in Figs 10–12 are 1·11, 1·25 and 2.51, respectively.

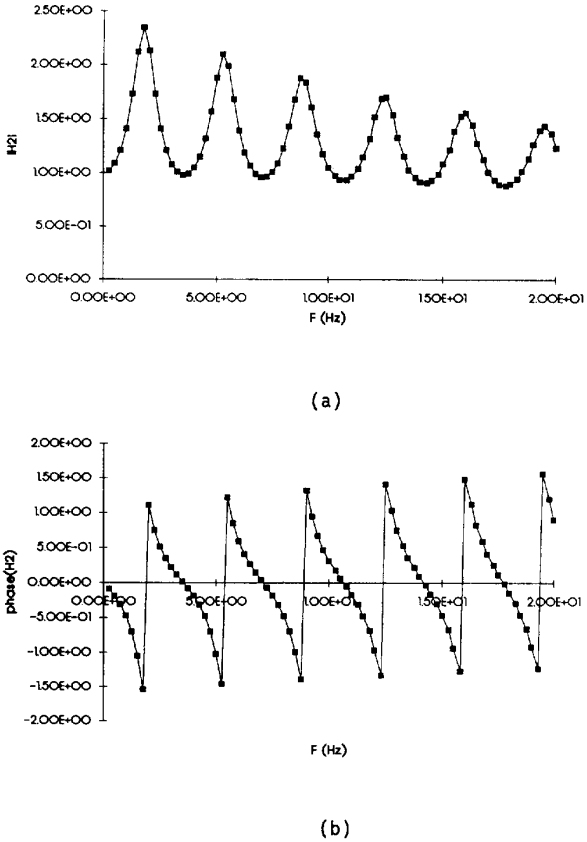


**Fig. 12.** Transfer function (a) amplitude and (b) phase angle for a two layered medium with $c_{top} = 0{\cdot}4c_{btm}$.

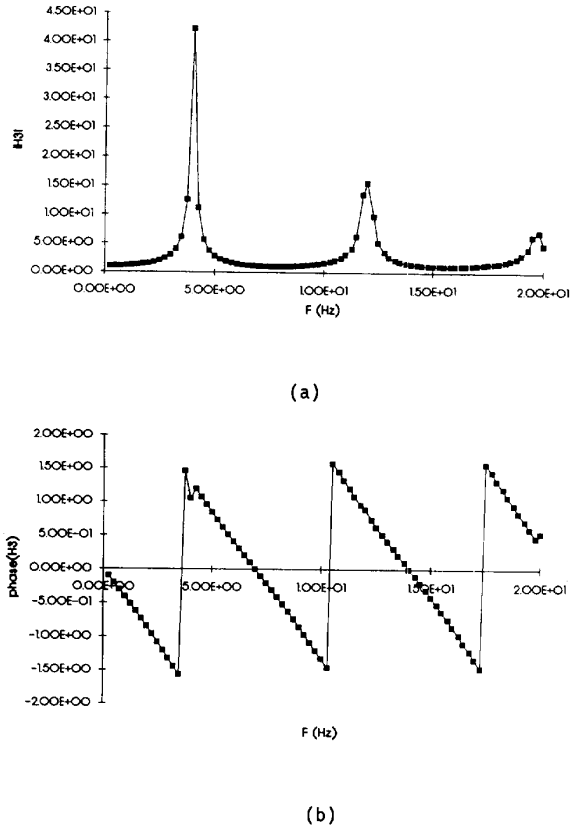


**Fig. 13.** Transfer function (a) amplitude and (b) phase angle for a three layered medium with $c_{top} = 0{\cdot}8c_{btm}$ and $c_{int} = 0{\cdot}9c_{btm}$.

Next, consider a configuration of two sandstone layers of depth $h_2 = h_1 = 100\,\mathrm{m}$ and wavespeeds $c_2 = 0{\cdot}8c_r$, $c_1 = 0{\cdot}9c_r$ resting on the same 'bedrock' as before [see Fig. 2(b)]. Figure 13 plots transfer function $H_3(f)$ amplitude and phase angle, while the relevant data needed in conjunction with eqn (43) are

$$R_2 = 0{\cdot}059 \qquad R_1 = 0{\cdot}053$$
$$\tau_2 = 0{\cdot}0705\,\mathrm{s} \qquad \tau_1 = 0{\cdot}0626\,\mathrm{s} \tag{62}$$

with $T = 0{\cdot}0089\,\mathrm{s}$ and $Q = 31{\cdot}42$ for both layers. The two-layer representation gives a different picture as compared to the single layer case with fewer eigenfrequencies ($f_k = 4{\cdot}5$, $13{\cdot}5$ and $19{\cdot}5\,\mathrm{Hz}$) in the 20 Hz range, which give very pronounced amplitude peaks.

## Comparison

The continuously inhomogeneous case, which is modelled through use of the Green's function approach, and the horizontally layered case, which is modelled through the transfer function approach, can now be compared for the sandstone layer with $c_{\mathrm{top}} = 0{\cdot}9c_{\mathrm{btm}}$ [Figs 7 and 9(a) vs. 10] and $c_{\mathrm{top}} = 0{\cdot}8c_{\mathrm{btm}}$ [Figs 8 and 9(b) vs 11]. At first, we see that the phase angle picture is very similar in all cases (homogeneous vs inhomogeneous, inhomogeneous vs layered) and we have four to five crossings of the frequency axis. As far as the amplitude picture is concerned, we observe the following differences: (i) there is no longer a one-to-one correspondence between the amplitude peaks and the phase angle crossings in the continuously inhomogeneous case, which means that the concept of layer eigenfrequencies does not exist; (ii) the amplitude curve does not decay with frequency in the inhomogeneous case as it does in the layered case (albeit at a very slow pace); (iii) as $f \to 0$, the layer transfer function always approaches unity which implies layer and bedrock move in unison under quasi-static conditions. This is

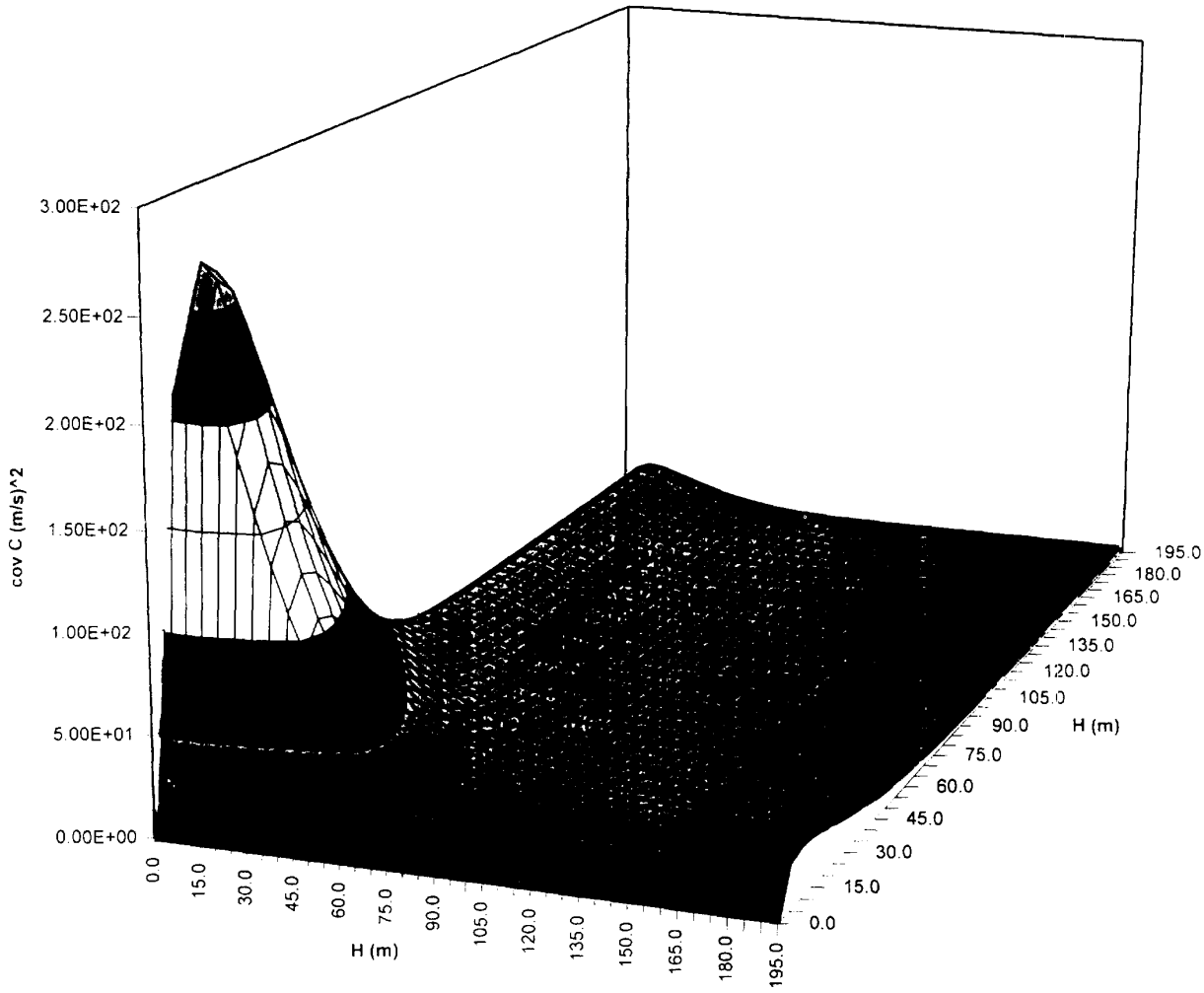


**Fig. 14.** Wavespeed covariance matrix for $\sigma_\gamma = 0{\cdot}1$ for the reference profile at $f = 1\,\mathrm{Hz}$.

not the case for a continuously inhomogeneous medium, since there is no discernible layer.

**Stochastic medium**

The effects of material stochasticity are next investigated in Figs 14 and 15, which respectively plot the covariances of the amplitudes of the local wavespeed and of the Green's function for the reference profile described earlier [see eqn (60)] and for $c_{top} = 0{\cdot}9c$) and at $f = 1$ Hz. The standard deviation of the random parameter $\gamma$ is taken as $\sigma_\gamma = 0{\cdot}1$ for both cases. Also, these covariances are computed up to the full layer depth of 200 m. We observe that the local wave speed covariance matrix is symmetrical and has a maximum relatively close to the free surface ($x_1 = x_2 = 10$ m), where the change in the mean wave speed profile is the sharpest (see Fig. 3). This maximum value implies a standard deviation for the wave speed which is 1·0% of the deterministic (or mean) value of the wave speed in that area. The covariance starts to decay rather quickly with increasing distance (as the corresponding mean wave speed profile becomes smoother), but remains nonzero throughout, indicating a fully correlated stochastic model. This is a consequence of the heterogeneous structure of the sandstone stratum considered herein.

The Green's function covariance matrix is also symmetric, remains constant for a large distance past the source and decays rather rapidly as the free surface is approached. This pattern corresponds to the mean Green's function amplitude profile (see Fig. 4), where the signal remains flat close to the source and changes rather quickly as the free surface ($x = 0$ or $R = 200$ m) is approached. The maximum standard deviation around the source corresponds to 0·4% of the deterministic (or mean) value of the signal amplitude in that region. Thus, the effect of stochasticity is less

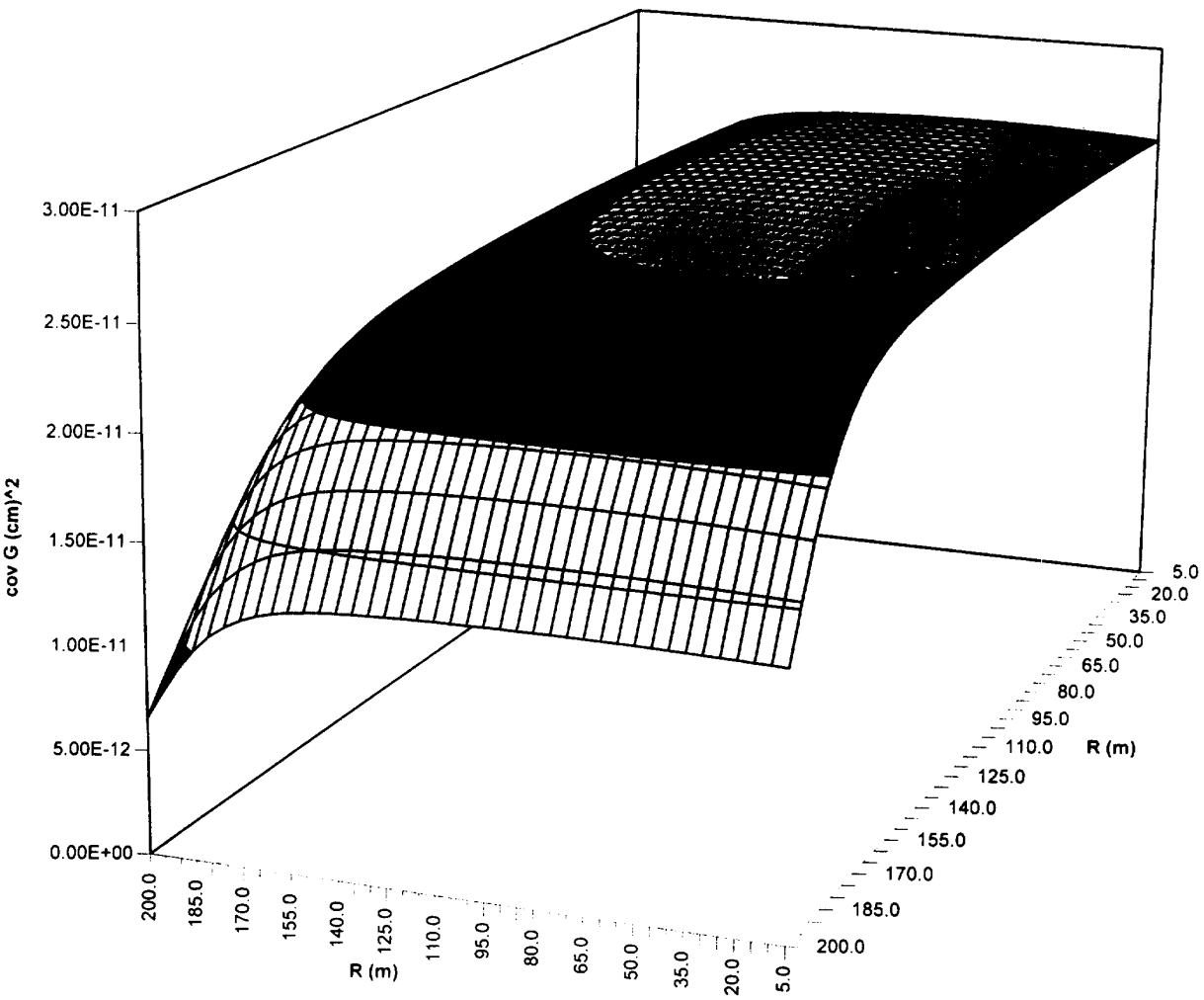


**Fig. 15.** Green's function covariance matrix for $\sigma_\gamma = 0{\cdot}1$ for the reference profile at $f = 1$ Hz.

pronounced in the signal amplitude as compared to the wave speed profile. Furthermore, the covariance remains nonzero throughout, indicating a fully correlated stochastic model. This conclusion was checked through normalization of the covariance matrix, which gave correlation coefficients equal to unity. Next, the Green's function covariance matrices for the reference case but at a higher level of inhomogeneity ($c_{top} = 0{\cdot}8c$) and at a higher frequency ($f = 10$ Hz) are respectively plotted in Figs 16 and 17. The former case is essentially a scaled version of the reference case, much like the situation observed for the corresponding mean values of the Green's function (see Figs 4 and 6). The latter case gives a rich surface profile with nodes where the covariance approaches zero which corresponds to the nearly zero amplitude points for the mean Green's function amplitude values of Fig. 5.

The results obtained for the Green's function by the present methodology are finally compared against the results of routine Monte Carlo simulations (MCS)[44] in Figs 18 and 19. Comparisons for the local wave speed yield similar conclusions and are omitted in the interest of brevity. Since the solution given by the present methodology is also the mean value predicted by first order perturbations, Fig. 18 first serves to gauge the level of agreement between the perturbation technique and the MCS, which were conducted for $N = 400$ samples at each spatial point. We observe a drift between the two sets of results as the radial distance increases, which approaches 10% at $R = 200$ m (the surface). Part of this drift is due, of course, to the fact that the mean stochastic solution is not equal to the deterministic one. This part, however, is deemed to be quite small since the variance specified for random parameter $\gamma$ is only 0·1. Most of the drift is due to round-off error in the particular MCS used herein, which was verified by reconstituting the mean and

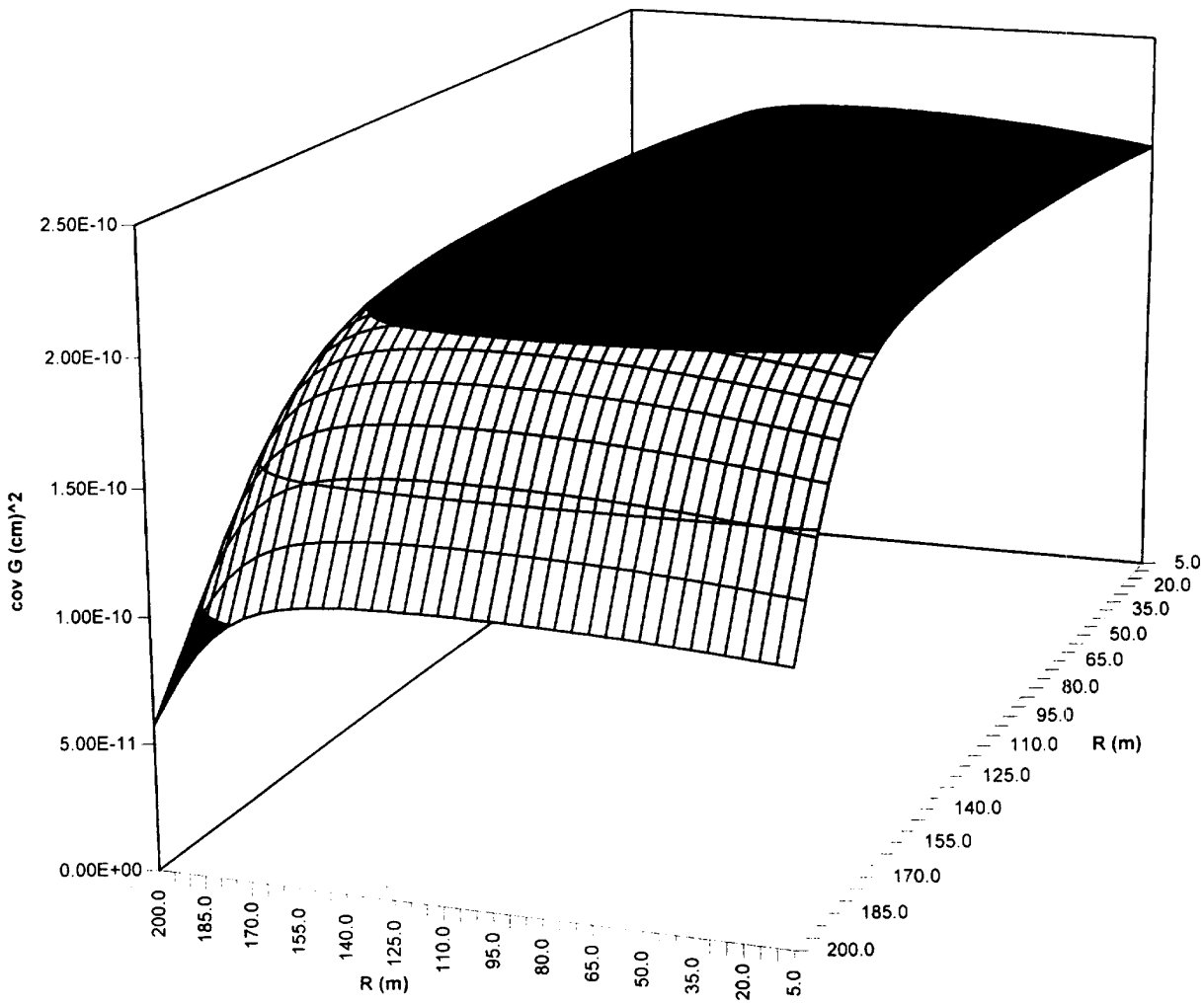


**Fig. 16.** Green's function covariance matrix for $\sigma_\gamma = 0{\cdot}1$ for the reference profile at $f = 1$ Hz but with $c_{top} = 0{\cdot}8c$.

variance of $\gamma$ from its realizations. This error in the mean values implies that there will be a divergence in the MCS for the covariance matrix at large $r$, since signal realizations will be subtracted from mean values at a particular grid point that have drifted from their reference position. As shown in Fig. 19, this is indeed the case: the percentage error is negligible and of the order of a few percentage points in the region close to the origin, but grows rapidly past 50 m for the source. This distance corresponds to the onset of detectable error in the Green's function mean amplitude simulations of Fig. 18. Since the error in the covariance simulations grows more rapidly than that in the mean value simulations, Fig. 19 plots up to $R = 100$ m from the source, where an error level of 10% has already been reached. Finally, as was discussed in Ref. 10, MCS are an order of magnitude more time consuming as compared to the perturbation approach.

## CONCLUSIONS

This work presented a Green's function approach for wave propagation in a continuously inhomogeneous medium, given time harmonic conditions and under the assumption that the material parameters of the problem vary in one principle direction only. The Green's function is obtained through an algebraic transformation technique. As such, it depends on *a priori* established relations between elastic modulus and density which, however, lead to realistic local wave speed profiles. Furthermore, the presence of a traction-free horizontal surface is accounted for by the method of images.

The Green's function is a versatile tool that can be integrated within a boundary integral equation formulation so as to address wave scattering and diffraction problems in inhomogeneous media. Furthermore,

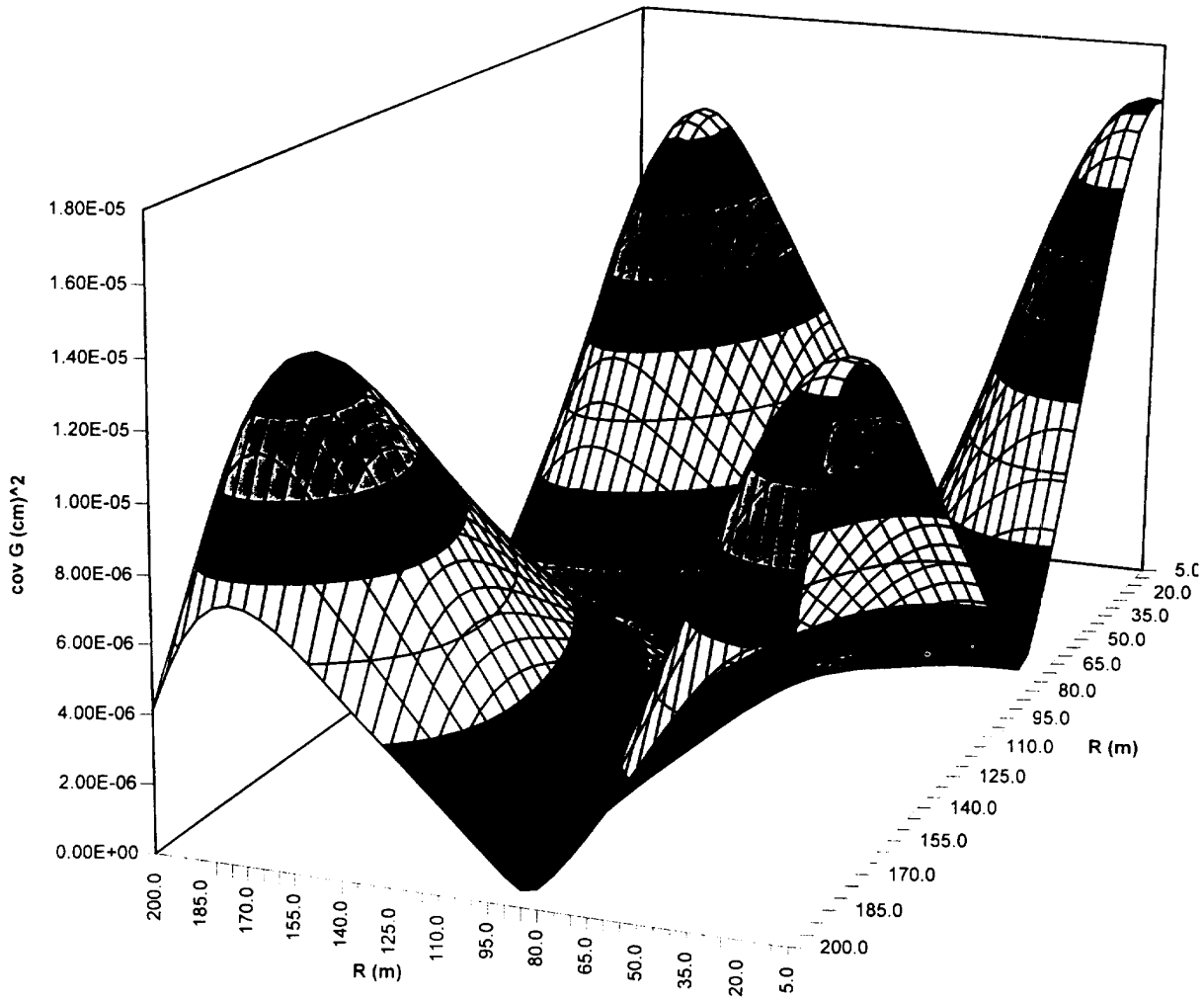


**Fig. 17.** Green's function covariance matrix for $\sigma_\gamma = 0{\cdot}1$ for the reference profile at $f = 10$ Hz.

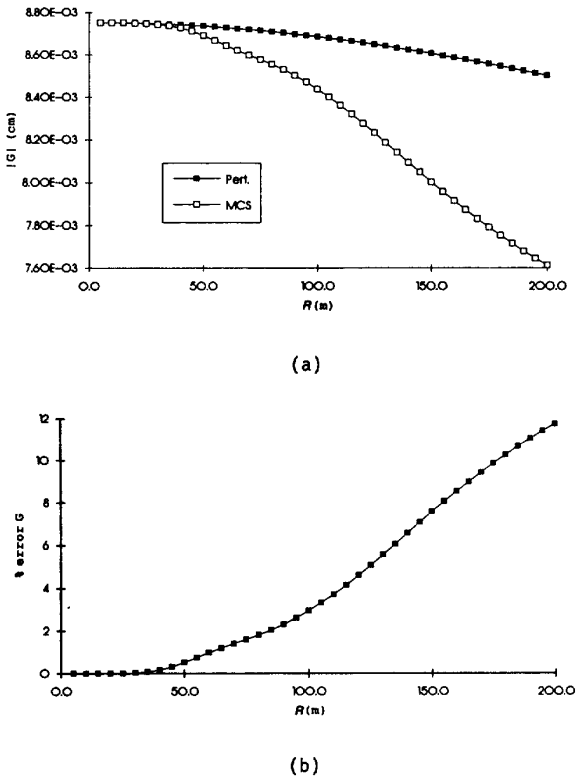


**Fig. 18.** (a) Amplitude and (b) percentage error in the Green's function mean value as computed by the present method and by MCS for the reference profile at $f = 1$ Hz.

when appropriately normalized, it can serve as a transfer function for wave propagation through a continuously inhomogeneous soil deposit. It can therefore be used as an alternative to conventional transfer functions for horizontally layered media, and especially for cases where layer interfaces are not clearly defined.

Next, randomness was introduced in the Green's

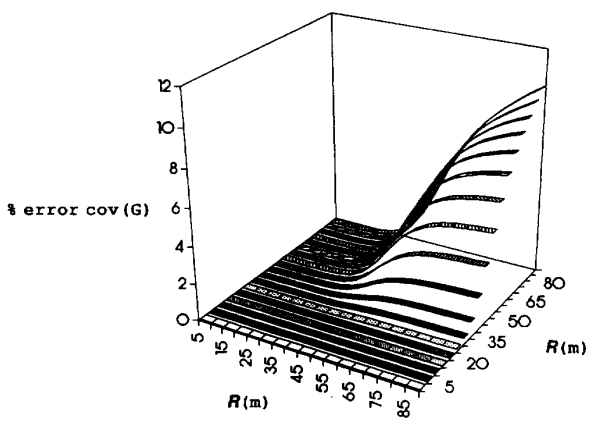


**Fig. 19.** Percentage error (absolute value) in the Green's function covariance matrix as computed by the present method and by MCS for the reference profile at $f = 1$ Hz.

functions and, through the use of the perturbation method, fundamental solutions were developed for the case of one-dimensional wave propagation in a stochastic heterogeneous medium. These results, which were in the form of mean values and covariances, were used to examine seismic wave propagation through geological media whose material parameters are both position-dependent and fluctuate about their mean values. Furthermore, these results were compared against standard Monte Carlo simulations that are almost two orders of magnitude more computationally involved than the present approach. Finally, the methodology is also applicable to vector wave propagation through the use of Helmholtz's decomposition of the displacement field into dilatational and rotational components. Thus, complete seismically-induced ground vibrations that include both pressure and shear waves can be examined.

## ACKNOWLEDGEMENT

We dedicate this work to Professor Franz Ziegler on the occasion of his 60th birthday.

## REFERENCES

1. Bard, P. Y. Effects of surface geology on ground motions: Recent results and remaining issues. In *10th European Conference on Earthquake Engineering*, ed. G. Duma. Balkema, Rotterdam, 1995, pp. 305–323.
2. Aki, K. & Richards, P. G. *Quantitative Seismology, II.* W. H. Freeman, San Francisco, CA, 1980.
3. Sheriff, R. E. & Geldart, L. P. *Exploratory Seismology, Vol. 1, History, Theory and Data Acquisition.* Cambridge University Press, Cambridge, 1982.
4. Ben-Menachem, A. & Singh, S. J. *Seismic Waves and Sources.* Springer-Verlag, Berlin, 1981.
5. Haskell, N. A. The dispersion of surface waves on multilayered media. *Bull. Seism. Soc. Amer.*, 1953, **71,** 2071–95.
6. Deodatis, G. & Theoharis, A. P. Seismic ground motion in a layered half-space due to a Haskell-type source. I: Theory, II: Applications. *Soil Dyn. Earthqu. Engng*, 1994, **13,** 281–92 and 293–301.
7. Chen, J. T., Chen, L. Y. & Hong, H. K. Regularization method for deconvolution problems in soil dynamics. In *Boundary Elements XVII Conference*, ed. C. A. Brebbia *et al.* Computational Mechanics Publications, Southampton, 1995, pp. 351–8.
8. Safak, E. Discrete time analysis of seismic site amplification. *J. Engng Mech. ASCE*, 1995, **121,** 801–9.
9. Vrettos, C. Dispersive SH-surface waves in soil deposits of variable shear modulus. *Soil Dyn. Earthqu. Engng*, 1990, **9,** 255–64.
10. Manolis, G. D. & Shaw, R. P. Wave motions in stochastic heterogeneous medi: a Green's function approach. *Engng Anal. Bound. Elem.*, 1995, **15,** 225–34.
11. Taylor, C. A., Dar, A. R. & Crewe, A. J. Shaking table modelling of seismic geotechnical problems. In *10th European Conference on Earthquake Engineering*, ed. G. Duma. Balkema, Rotterdam, 1995, pp. 441–6.

12. Clouteau, D. & Aubry, D. Site effects on 3D elevated topography. In *Soil Dyn. Earthq. Engng. VII Conf.*, ed. A. S. Cakmak & C. A. Brebbia. Computational Mechanics Publications, Southampton, 1995, pp. 291–8.
13. Mossessian, T. K. & Dravinski, M. Scattering of elastic waves by three-dimensional surface topographies. *Wave Motion*, 1989, **11**, 579–92.
14. Luco, J. E., Wong, H. L. & De Barros, F. C. P. Three dimensional response of a cylindrical canyon in a layered halfspace. *Earthqu. Engng Struct. Dyn.*, 1990, **19**, 799–817.
15. Wen, K. L. Nonlinear soil response in ground motion. *Earthqu. Engng Struct. Dyn.*, 1994, **23**, 599–608.
16. Bonnet, G. & Heitz, J. F. Nonlinear seismic response of a soft layer. In *10th European Conf. Earthquake Engng*, ed. G. Duma. Balkema, Rotterdam, 1995, pp. 361–4.
17. Liambias, J. M., Shepherd, D. J. & Bousfield, J. P. A comparison of equivalent linear and nonlinear approaches for site amplification studies. In *Struct. Mech. in Reactor Tech. '89 Conference, Vol. K1*, ed. A. H. Hadjian. SMIRT Publication, Anaheim, CA, 1989, pp. 73–8.
18. Wolf, J. P. *Dynamic Soil-Structure Interaction*. Prentice-Hall, Englewood Cliffs, NJ, 1985.
19. Ewing, W. M., Jardetzky, W. S. & Press, F. *Elastic Waves in Layered Media*. McGraw-Hill, New York, 1957.
20. Pires, J. A. Stochastic seismic response analysis of soft soils. In *Struct. Mech. in Reactor Tech. 12 Conference, Vol. MK02*, ed. K. Kussmaul. Elsevier Science Publishers, London, 1993, pp. 214–24.
21. Kausel, E. & Roesset, J. M. Modelling hysteretic damping. In *10th European Conf. Earthquake Engng*, ed. G. Duma. Balkema, Rotterdam, 1995, pp. 1229–34.
22. Manolis, G. D. & Shaw, R. P. Harmonic wave propagation through viscoelastic heterogeneous media exhibiting mild stochasticity, Parts I and II. *Soil Dyn. Earthqu. Engng*, 1995, **15**, 119–127 and 129–139.
23. Ambraseys, N. N. & Srbulov, M. Attenuation of earthquake-induced ground displacements. *Earthqu. Engng Struct. Dyn.*, 1994, **23**, 467–87.
24. Klimis, N. S. Laboratory identification of the quality factor *Q*: comparative presentation and evaluation of spectral ratio and rise time methods. In *Soil Dynamics Earthquake Engineering VII Conference*, ed. A. S. Cakmak & C. A. Brebbia. Computational Mechanics Publications, Southampton, 1995, pp. 424–32.
25. Skipp, B. O. Acquisition, choice and use of ground parameters for soil–structure interaction analysis. In *Proc. 10th Europ. Conf. Earthqu. Engng*, ed. G. Duma. Balkema, Rotterdam, 1995, pp. 425–40.
26. Borcherdt, R. D. Estimates of site-dependent response spectra for design, methodology and justification. *Earthqu. Spectra*, 1994, **10**, 617–53.
27. Shinozuka, M., Deodatis, G. & Harada, T. Digital simulation of seismic ground motion. In *Stochastic Approaches in Earthquake Engineering*, ed. Y. K. Lin *et al.*, Springer-Verlag, Berlin, 1987, pp. 252–98.
28. Ramadan, O. & Novak, M. Simulation of multidimensional anisotropic ground motions. *J. Engng Mech. ASCE*, 1994, **120**(8), 1773–85.
29. Manolis, G. D. The ground as a random medium. In *Boundary Element Techniques in Geomechanics*, Chapter 15, ed. G. D. Manolis & T. G. Davies. Elsevier Applied Science, London, 1993.
30. Kiyono, J., Toki, K. & Sato, T. Development of stochastic discrete wave-number method for seismic response analysis of ground with irregular interfaces. In *Earthquake Resistant Construction and Design, Vol. 1*, ed. S. Savidis. Balkema, Rotterdam, 1994, pp. 69–76.
31. Aki, K. & Larner, K. L. Surface motion of layered media having an irregular interface due to incident plane SH wave. *J. Geophys. Res.*, 1970, **75**, 933–54.
32. Vanmarke, E., Shinozuka, M., Nakagiri, S., Schueller, G. I. & Grigoriu, M. Random fields and stochastic finite elements. *Struct. Safety*, 1986, **3**, 143–66.
33. Liu, W. K., Belytschko, T. & Mani, A. Random field finite elements. *Int. J. Num. Meth. Engng*, 1986, **23**, 1831–45.
34. Wu, Z. & Han, G. Stochastic seismic response analysis for soil layers with random dynamic parameters. In *Proc. 10th World Conf. Earthqu. Engng, Vol. 2*, Madrid, Spain. Balkema, Rotterdam, 1992, pp. 1187–92.
35. Grundmann, H. & Waubke, H. Approximate solution for the response of a layered stochastic linear soil to a dynamic excitation at the surface. In *Structural Dynamics, Proc. EURODYN '93 Conference*, Trodheim, Norway, ed. C. Moan *et al.* Balkema, Rotterdam, 1993, pp. 713–20.
36. Suzuki, S. & Asano, K. Dynamic application functions of the surface layer considering the variation of soil parameters. In *Proc. 10th World Conf. Earthqu. Engng, Vol. 2*, Madrid, Spain. Balkema, Rotterdam, 1992, pp. 1193–8.
37. Ghanem, R. G. & Spanos, P. D. *Stochastic Finite Elements: A Spectral Approach*. Springer-Verlag, Berlin, 1991.
38. Waubke, H. & Grundmann, H. A spectral approach for the stochastic local soil response. In *Earthquake Resistant Construction and Design, Vol. 1*, ed. S. Savidis. A. A. Balkema, Rotterdam, 1994, pp. 101–8.
39. Manolis, G. D. & Beskos, D. E. *Boundary Element Methods in Elastodynamics*. Unwin-Hyman (Chapman and Hall), London, 1988.
40. Shaw, R. P. & Makris, N. Green's functions for Helmholtz and Laplace equations in heterogeneous media. *Engineering Analysis with Boundary Elements*, 1992, **10**, 179–83.
41. Vladimirov, V. S. *Equations of Mathematical Physics*. MIR Publishers, Moscow, 1983.
42. Christiansen, R. M. *Theory of Viscoelasticity, an Introduction*. Academic Press, San Diego, CA, 1982.
43. Safak, E. A new model to simulate site effects. In *10th European Conference on Earthquake Engineering*, ed. G. Duma. Balkema, Rotterdam, 1995, pp. 297–303.
44. Press, W. H., Flannery, S. A., Teukolsky, S. A. & Vetterling, W. T. *Numerical Recipes*. Cambridge University Press, Cambridge, 1989.